Society of Medical Education & Research

2026, Volume 6, Issue 1, Page No: 21-38

ISSN: 3108-4834

Archive of International Journal of Cancer and Allied Science

A Long Non-coding RNA-Based Predictive Model for Peritoneal Recurrence after Radical Gastrectomy in Patients with Gastric Cancer

Santiago Morales[1]*, Laura Rojas[2], Camila Vega[1], Diego Molina[3]

[1]Department of Gastric Cancer and Peritoneal Recurrence, Faculty of Medicine, University of Buenos Aires, Buenos Aires, Argentina.

[2]Department of Predictive Modeling and Long Noncoding RNA, Faculty of Medicine, Pontifical Catholic University of Chile, Santiago, Chile.

[3]Department of Surgical Oncology and Radical Gastrectomy, Faculty of Medicine, National University of La Plata, La Plata, Argentina.

***E-mail** ✉ santiago.morales@med.uba.ar

Abstract

Long non-coding RNAs (lncRNAs) exert substantial influence on the development and metastatic spread of gastric cancer (GC). Despite this, systematic studies using tissue-derived lncRNAs to predict peritoneal recurrence in GC patients remain insufficient. The current investigation aims to delineate the lncRNA transcriptional profile in GC with peritoneal metastasis (PM) and to develop an integrated lncRNA-derived scoring system to predict peritoneal recurrence in individuals undergoing radical gastrectomy. Transcriptomic analysis of lncRNAs was conducted on matched samples of peritoneal tissue, primary gastric tumors, and adjacent normal tissues collected from 12 GC patients within the Sun Yat-sen University Cancer Center (SYSUCC) discovery set. Candidate lncRNAs were pinpointed by cross-referencing findings with the TCGA database and an independent SYSUCC validation cohort. A prognostic risk model was generated through LASSO regression, followed by construction of a nomogram based on Cox proportional hazards regression. The model's discriminatory performance was evaluated using receiver operating characteristic (ROC) curve analysis. The functional effects of lncRNAs on PM were subsequently validated using wound-healing assays, Transwell migration/invasion assays, three-dimensional multicellular tumor spheroid invasion models, and in vivo peritoneal xenograft experiments in mice. Five pivotal lncRNAs were identified and assembled into a PM risk score designed to estimate peritoneal recurrence-free survival (pRFS). An integrated nomogram combining this PM risk score with pT stage, pN stage, and tumor size was established, achieving robust prediction of 5-year pRFS with an area under the curve of 0.79 (95% CI: 0.71-0.88). Functional experiments further showed that CASC15, one of the selected lncRNAs, significantly augmented the migratory and invasive abilities of GC cells in vitro and accelerated peritoneal dissemination in vivo. These findings provide direct evidence of lncRNA involvement in GC peritoneal metastasis. Mechanistic studies revealed that CASC15 drives epithelial-mesenchymal transition and metastatic behavior by activating the JNK and p38 signaling cascades. The present study developed an integrated lncRNA-based scoring tool to predict peritoneal recurrence in GC patients.

Keywords: Gastric cancer, Transcriptome profiles, Long non-coding RNA, Peritoneal recurrence

Introduction

Gastric cancer (GC) represents the fourth leading cause of cancer incidence worldwide. It is typically diagnosed at advanced stages due to its vague initial clinical manifestations, posing a major global health challenge [1, 2]. The peritoneal cavity is a predominant site of distant spread and disease relapse in GC, with profound clinical implications [2-4]. Patients who experience peritoneal metastases (PM) face markedly diminished survival outcomes, with median overall survival

Access this article online https://smerpub.com/

Received: 25 October 2025; **Accepted:** 20 January 2026

How to cite this article: Morales S, Rojas L, Vega C, Molina D. A Long Non-coding RNA-Based Predictive Model for Peritoneal Recurrence after Radical Gastrectomy in Patients with Gastric Cancer. Arch Int J Cancer Allied Sci. 2026;6(1):21-38. https://doi.org/10.51847/0FScHYFYBf

generally less than 6 months [5]. Early recognition of high-risk individuals is therefore of paramount importance.

Although computed tomography (CT) and positron emission tomography (PET) are widely applied for PM detection in GC [6, 7], their diagnostic sensitivity and precision remain inadequate [6, 8, 9]. Laparoscopic exploration with histopathological confirmation remains the reference standard [7]; however, its invasive nature limits its routine use in the broader GC population. Hence, the identification of precise, noninvasive biomarkers for PM risk stratification is both urgently needed and highly valuable in clinical practice.

Long non-coding RNAs (lncRNAs), transcripts surpassing 200 nucleotides in length, participate in diverse regulatory mechanisms including transcriptional control, chromatin organization, and post-transcriptional modulation [10, 11]. Their frequent display of cell- or tissue-specific expression patterns positions them as promising candidates for disease biomarkers [12]. For example, Zhou *et al*. [13] characterized malignancy-related lncRNAs in esophageal squamous cell carcinoma (ESCC) and highlighted their applicability as noninvasive tools for early ESCC screening. In the context of GC, multiple lncRNAs are associated with peritoneal metastasis. Dong *et al*. [14] observed upregulation of lnc-TRIM28-14 in PM lesions, thereby improving diagnostic accuracy for GC with peritoneal involvement. Similarly, Wang *et al*. [15] reported that nanoparticle-delivered LINC00589 effectively restrained PM formation both in vitro and in vivo. These molecules not only aid therapeutic decision-making but also hold potential as targets for personalized interventions.

Nevertheless, large-scale analyses of tissue-derived lncRNAs for predicting peritoneal recurrence in GC remain notably limited. Accordingly, this study was undertaken to characterize the lncRNA transcriptome in GC with PM and to construct a composite lncRNA-based predictive score for peritoneal recurrence risk after radical gastrectomy.

Within this work, lncRNA expression profiles were examined in paired peritoneal, primary tumor, and normal tissues from 12 GC patients. Integration with TCGA data and the SYSUCC validation cohort enabled selection of five key lncRNAs. These were combined to generate a PM risk score for forecasting peritoneal recurrence-free survival (pRFS), with higher scores indicating a higher recurrence probability. A multifaceted nomogram integrating the PM risk score, pT category, pN category, and tumor diameter was subsequently developed. This nomogram demonstrated strong performance in predicting pRFS, recurrence-free survival (RFS), and overall survival (OS), while also stratifying patients by potential benefit from adjuvant chemotherapy. In-depth functional evaluation of CASC15 confirmed its promotion of GC cell metastatic potential in vitro and peritoneal colonization in vivo, thereby corroborating the role of lncRNAs in GC peritoneal metastasis. In conclusion, the lncRNA-integrated scoring system introduced here offers significant promise for personalized clinical assessment of peritoneal recurrence risk in GC.

Materials and Methods

Collection and preparation of patient specimens

The present research was carried out in full adherence to the principles outlined in the Declaration of Helsinki and received ethical clearance from the Institutional Review Board (IRB) of Sun Yat-Sen University Cancer Center (SYSUCC, Guangzhou, China), with approval number G2021-036. Matched specimens consisting of normal gastric mucosa, primary gastric tumors, and peritoneal metastatic (PM) tissues were obtained from 12 GC patients diagnosed with PM at SYSUCC for subsequent transcriptome sequencing. These patients had developed tumor-related hemorrhage or obstruction, necessitating palliative gastrectomy. In addition, 231 patients with pathologically confirmed stage II or III GC who received radical gastrectomy without prior chemotherapy or radiotherapy were included in the SYSUCC validation cohort, with enrollment spanning December 2013 to December 2016. Eligible participants were adults aged 18 years and above of either sex, possessing a minimum life expectancy of 3 months and adequate follow-up records. Individuals with any prior malignancy within the last 5 years were excluded. Fresh tumor tissues were snap-frozen immediately after collection at SYSUCC. Relevant clinical and histopathological information was extracted via retrospective analysis of electronic medical records, supplemented by long-term outcome data from the institutional follow-up unit. All patients provided written informed consent before participation.

High-throughput data processing and lncRNA expression mining

RNA sequencing of peritoneal metastasis-associated samples from the SYSUCC GC cohort was performed on

the HiSeq 4000 sequencing platform (Illumina, Inc., San Diego, CA, USA). Pre-processed RNA-seq datasets for gastric cancer tissues from the TCGA project were retrieved from the UCSC Xena browser (http://xena.ucsc.edu/). Gene expression quantification was performed using transcripts per million (TPM) values for all downstream analyses.

LASSO regression analysis and PM risk score establishment

Least absolute shrinkage and selection operator (LASSO) regression was implemented to screen candidate lncRNAs and construct a peritoneal metastasis (PM) risk score. This method applies an L1 regularization penalty to drive less contributory coefficients toward zero. The regularization parameter λ governs the degree of shrinkage applied. In the current analysis, λ was gradually reduced to moderate the penalty and retain more variables. Optimal λ selection was achieved via 200-fold cross-validation, using the 1-standard-error (SE) rule. The PM risk score for individual patients across the SYSUCC and TCGA cohorts was then derived using the equation: PM risk score = ∑exp(i) * coef(i), in which exp(i) indicates the expression value of each lncRNA and coef(i) corresponds to its LASSO-derived coefficient.

Cell culture

Human gastric cell lines GES1, AGS, SNU216, HGC27, SNU719, MKN28, and BGC823 were maintained in RPMI1640 or DMEM (Invitrogen, Carlsbad, USA) supplemented with 10% fetal bovine serum (FBS; Gibco, NY, USA). Cultures were incubated at 37 °C under a 5% CO_2 atmosphere in standard culture dishes (JET BIOFIL, Guangzhou, China). All lines were confirmed negative for *Mycoplasma* infection.

Antibodies and chemicals

The primary antibodies utilized were: E-Cadherin (BD Biosciences 610182, IB dilution 1:1000), N-Cadherin (BD Biosciences 610921, IB dilution 1:1000), β-catenin (Proteintech 51067, IB dilution 1:3000), Vimentin (Proteintech 60330, IB dilution 1:2000), α-smooth muscle actin (Proteintech 14395, IB dilution 1:2000), p38 (Cell Signaling Technology (CST) 9212, IB dilution 1:1000), Phospho-p38 (Cell Signaling Technology (CST) 4511, IB dilution 1:1000), JNK (Cell Signaling Technology (CST) 9252, IB dilution 1:1000), Phospho-JNK (Cell Signaling Technology (CST) 9255, IB dilution 1:1000), ERK1/2 (Cell Signaling Technology (CST) 4695, IB dilution 1:1000), Phospho-ERK1/2 (Cell Signaling Technology (CST) 4370, IB dilution 1:1000), and GAPDH (Proteintech 60004, IB dilution 1:1000). The pharmacological agents included Anisomycin (Selleck Chemistry S7409), SB203580 (Selleck Chemistry S1076), and SP600125 (Selleck Chemistry S1460).

Generation of stable cell lines

Expression plasmids for CASC15 overexpression together with short hairpin RNA constructs (sh1 target sequence: TTGGCAGTCACACTTGGACTC; sh2 target sequence: AAGAAATCAAGCCTGCCCATA) were sourced from TSINGKE (Guangzhou, China). Lentiviruses were packaged through simultaneous transfection of these plasmids with helper vectors psPAX2 and pMD2.G into HEK293T cells facilitated by JetPrime transfection reagent (Polyplus, France). Harvested viral supernatants were applied to infect recipient cells and establish stable lines. Puromycin selection was performed for several days post-transduction. Quantitative RT-PCR validated knockdown or overexpression efficacy. For in vivo bioluminescence tracking, cells were further modified with lentiviral constructs carrying Gaussia luciferase (Gluc) and selected under geneticin pressure.

Quantitative RT-PCR

Total RNA was isolated from cell cultures or tissue specimens employing TRIzol reagent (Invitrogen, Carlsbad, CA, USA), followed by reverse transcription into cDNA using a Reverse Transcription Kit (TAKARA, Beijing, China). Real-time PCR amplification was performed with SYBR Green SuperMix (Roche, Basel, Switzerland), and expression data were normalized to the housekeeping gene GAPDH.

Western Blotting

Harvested cells were disrupted on ice for 30 min utilizing a lysis buffer containing 50 mM Tris-HCl (pH 7.4), 150 mM NaCl, 1 mM EDTA, 0.5% NP-40, and 10% glycerol, supplemented with a protease inhibitor cocktail (CW2200S, CWBIO, China). Protein quantification was achieved with the BCA Protein Assay Kit (GLPBIO, GK10009). Lysates were mixed with SDS loading buffer and boiled at 100 °C for 10 min. Proteins were resolved by SDS-PAGE electrophoresis and transferred electrophoretically onto polyvinylidene fluoride

membranes. After blocking in 5% non-fat milk, membranes were probed with appropriate primary and secondary antibodies. Chemiluminescent signals were captured using the ChemiDoc Touch imaging system (Bio-Rad, USA).

Transwell assays

Cells suspended in 100 µL serum-free RPMI1640 medium (5×10^4 cells for invasion assays or 2×10^4 cells for migration assays) were placed into the upper chamber of 24-well Boyden inserts, either uncoated or pre-coated with Matrigel (BD Biosciences, New Jersey, USA). The lower compartment contained medium supplemented with 20% serum. Following 24 h incubation, cells remaining on the upper membrane surface were removed. Migrated or invaded cells on the lower surface were fixed in methanol at ambient temperature, stained with crystal violet, and enumerated via microscopic imaging.

Wound-healing assay

Gastric cancer cells were plated uniformly in 6-well dishes and grown to near-confluence overnight. Monolayers were then scratched with a 200-µL pipette tip to generate linear wounds. After PBS rinsing to clear debris, serum-free medium was introduced. Initial images were recorded as reference points under a microscope. Following an additional 24 h of culture, photographs were reacquired at identical positions to assess wound closure rates.

Cell proliferation detection

Cells were plated at 2×10^3 cells per well in 96-well microtiter plates and maintained in standard culture conditions. Proliferative capacity was evaluated at 24-hour intervals by adding the CCK-8 reagent (MCE, Shanghai, China) and measuring absorbance according to the manufacturer's guidelines.

Colony formation assay

Trypsin-dissociated cells were seeded at densities of 500–1000 cells per well into 6-well plates. After overnight attachment, cultures were continued in standard growth medium or with designated treatments for 10–14 days to allow colony development. Resulting colonies were fixed with methanol for 20 min at room temperature, stained with 0.5% crystal violet solution for 2 h, rinsed thoroughly, and air-dried. Whole plates were imaged using a ChemiDoc Touch system (Bio-Rad, USA), and colony areas were measured with ImageJ software.

3D multicellular tumor spheroids invasion assay

Three-dimensional co-culture models were established according to a previously reported protocol [16]. In short, 1×10^4 gastric cancer cells were suspended and embedded within growth medium containing 2% Matrigel. The culture medium was renewed every 2 days for 7 days. Bright-field microscopy images were captured using Olympus CellSens Standard 1.9 software, and the invaded regions were quantified.

In-Situ Hybridization (ISH) staining

A commercial ISH detection kit targeting human lncRNA CASC15 was acquired from Bioster-Bio (Wuhan, China). Procedures were conducted precisely as recommended by the manufacturer. Tissue sections underwent deparaffinization in xylene, graded rehydration, and pepsin digestion. Hybridization with digoxin-labeled probes was carried out overnight. Subsequent signal detection involved incubation with a streptavidin-horseradish peroxidase conjugate, followed by chromogenic development with 3,3′-diaminobenzidine (DAB).

Fluorescence In-Situ Hybridization (FISH) and phalloidin staining

A CY3-conjugated FISH probe specific for CASC15 was designed and synthesized by TSINGKE (Guangzhou, China). The RNA FISH procedure was executed using the RNA FISH Kit (GenePharma, China) following the supplier's instructions. For actin cytoskeleton visualization, cells grown on confocal dishes were fixed in 4% paraformaldehyde, permeabilized with 0.5% Triton X-100, and stained with phalloidin for 20 min. Nuclear counterstaining was achieved with 4′,6-diamidino-2-phenylindole. All fluorescence images were captured on an Olympus FV1000 confocal microscope (Tokyo, Japan).

Xenograft tumorigenicity assay in mice

Five-week-old female NSG or BALB/c nude mice were obtained from Vital River Laboratory Animal Technology (Beijing, China) and randomly allocated to two or three experimental groups. Peritoneal tumor formation was induced by injecting 1×10^7 AGS cells or 6×10^6 SNU719 cells (suspended in 100 µL sterile PBS mixed with 20% high-concentration Matrigel matrix;

CORNING, NY, USA) into the abdominal cavity of BALB/c nude mice. In parallel, 5×10^6 MKN28 cells were administered intraperitoneally to NSG mice. Tumor progression was monitored at selected time points by intraperitoneal administration of 150 µL D-luciferin solution (15 mg/mL; GoldBio, cat. no. LUCK-1) and subsequent imaging with a Xenogen IVIS Lumina Series II system. All animals were humanely euthanized 4 weeks after cell inoculation.

Statistical analysis

Where appropriate, continuous variables were analyzed using unpaired two-sided Student's t-tests or Mann-Whitney U tests. Categorical data were evaluated with χ^2 tests or Fisher's exact tests. Survival outcomes, including peritoneal recurrence-free survival (pRFS), recurrence-free survival (RFS), and overall survival (OS), were estimated using the Kaplan-Meier method, and group differences were assessed using the log-rank test. Hazard ratios were derived from Cox proportional hazards regression models. Statistical computations were performed in the R environment (version 4.3.2). LASSO regression was implemented using the "glmnet" package, and nomograms were generated with the "rms" package. Model performance was evaluated by constructing receiver operating characteristic (ROC) curves and calculating the area under the curve (AUC). The 95% confidence intervals around AUC estimates were obtained using the "timeROC" package. Survival-related analyses employed the "survminer" package. All functional experiments were independently repeated at least three times, and data from one representative experiment are displayed. Results are reported as mean ± standard deviation (S.D.). Differences between groups were considered statistically significant at $P < 0.05$, as determined by two-tailed Student's t-test or two-way ANOVA.

Results and Discussion

Identification of lncRNA expression profiles in gastric cancer with peritoneal metastasis

This investigation employed a multi-platform clinical approach that integrated discovery and validation phases to identify lncRNA biomarkers for predicting peritoneal metastasis (PM) **(Figure 1a)**. In the discovery stage, genome-wide screening was performed on specimens from the Sun Yat-sen University Cancer Center (SYSUCC) cohort. The analyzed samples consisted of matched pairs of normal gastric mucosa, primary gastric carcinomas, and peritoneal metastatic deposits derived from 12 patients with gastric cancer (GC) accompanied by PM. A heatmap **(Figure 1b)** shows the lncRNAs with differential expression across these tissue groups. Volcano plots further delineate the significantly altered lncRNAs comparing normal gastric tissue to primary tumors **(Figure 1c)** and normal gastric tissue to PM tissues **(Figure 1d)**. To select lncRNAs potentially relevant to clinical outcomes, transcriptomic datasets from 414 GC cases in the TCGA database—encompassing primary tumor and matched adjacent normal tissues—were interrogated, leading to the nomination of 10 candidate lncRNAs. In parallel, transcript abundance of the 10 lncRNAs was quantified in normal gastric tissue, primary tumors, and PM lesions **(Figure 1e)**. Collectively, these preliminary observations highlight the potential utility of these 10 lncRNAs in predicting peritoneal dissemination and overall prognosis.

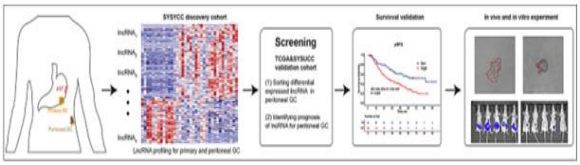

a)

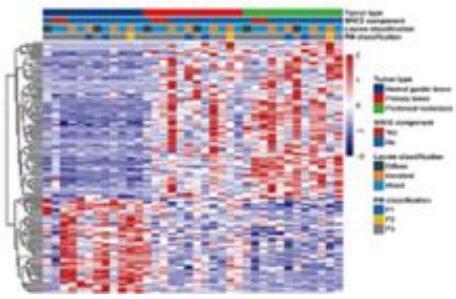

b)

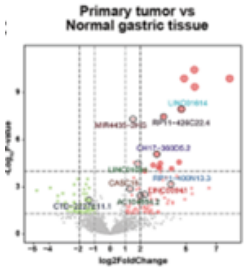

c)

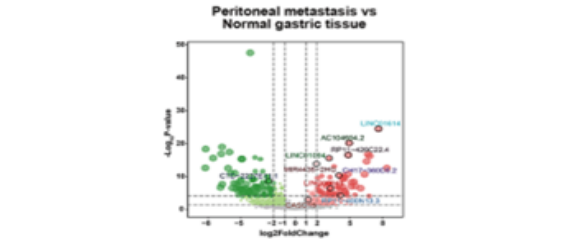

d)

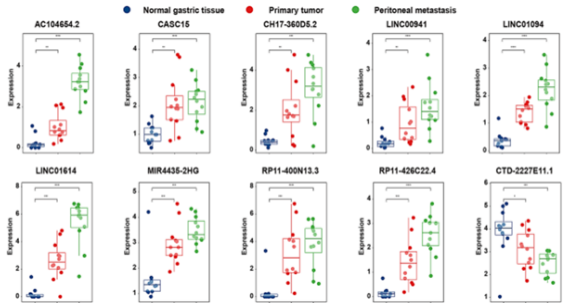

e)

Figure 1. Identification of lncRNA Expression Profiles in Gastric Cancer with Peritoneal Metastasis

(a) Schematic diagram outlining the experimental workflow of the study, (b) Heatmap illustrating lncRNAs exhibiting distinct expression patterns across matched normal gastric mucosa, primary gastric carcinomas, and PM tissues sourced from the SYSUCC discovery cohort, (c) Volcano plot indicating the log2 (fold change) for lncRNAs showing statistically significant differential expression when contrasting primary gastric tumor tissue against normal gastric tissue, (d) Volcano plot indicating the log2 (fold change) for lncRNAs showing statistically significant differential expression when contrasting PM tissue against normal gastric tissue, and (e) Boxplots depicting expression abundance of the 10 lncRNAs in matched normal gastric tissue, primary gastric tumor, and peritoneal metastatic samples. Statistical analysis was conducted using the Mann-Whitney U test. *P < 0.05, **P < 0.01, ***P < 0.001, ****P < 0.0001. Abbreviations: SYSUCC, Sun Yat-sen University Cancer Center; TCGA, The Cancer Genome Atlas; lncRNA, long non-coding RNA; ANT, adjacent normal tissues; GC, gastric cancer; SRCC, signet-ring-cell carcinoma; PM, peritoneal metastasis

Genome-wide identification of lncRNAs associated with peritoneal metastasis

Specimens from 231 gastric cancer (GC) patients classified as pathological stages II or III following radical gastrectomy were gathered for analysis. Following RNA extraction from these tissues, the expression of the 10 candidate lncRNAs was quantified through quantitative RT-PCR. Patients were subsequently categorized into high- and low-expression subgroups based on optimally determined threshold values. LINC00941 was omitted from further evaluation among the 10 lncRNAs owing to its inadequate expression levels. Of the nine remaining lncRNAs, increased expression of seven specific transcripts—AC104654.2, CASC15, CH17-360D5.2, LINC01094, LINC01614, MIR4435-2HG, and RP11-400N13.3—was linked to poorer peritoneal recurrence-free survival (pRFS) **(Figure 2a)**. These associations were summarized in a forest plot, while the capacity of all nine lncRNAs to predict recurrence-free survival (RFS) and overall survival (OS) was additionally examined.

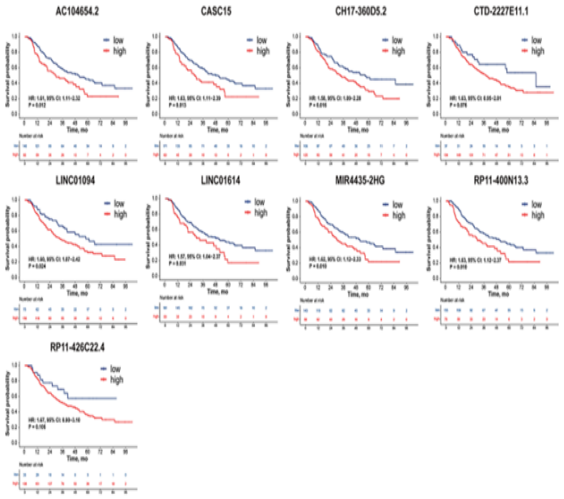

a)

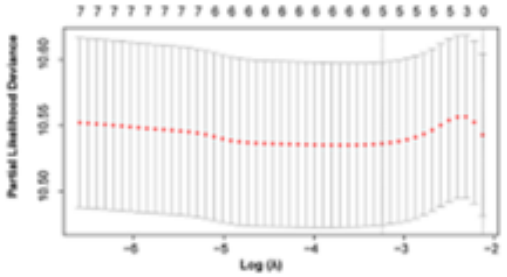

b)

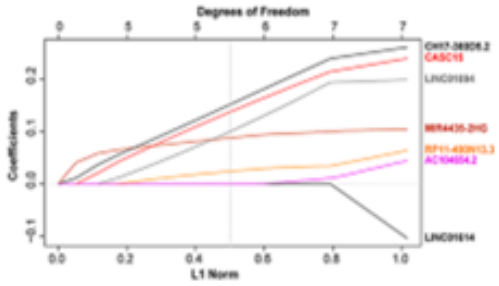

c)

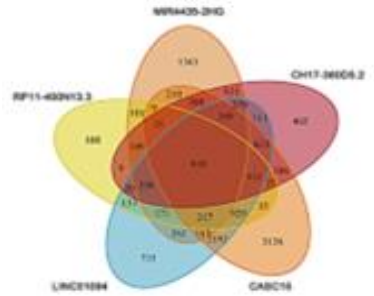

d)

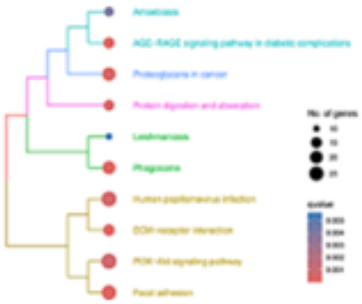

e)

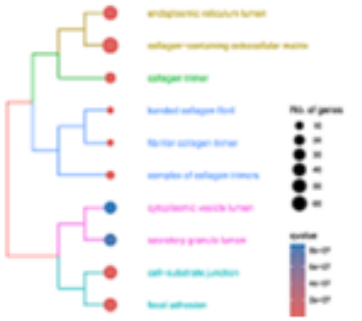

f)

Figure 2. Genome-wide Identification of Peritoneal Metastasis-Associated lncRNAs

(a) Kaplan-Meier curves depicting peritoneal recurrence-free survival (pRFS) according to high versus low expression of the nine lncRNAs in the SYSUCC validation cohort, as determined by quantitative RT-PCR, (b) Partial likelihood deviance plot for the seven lncRNAs selected via the LASSO regression model, with tuning parameter optimization performed through 200-fold cross-validation, (c) LASSO coefficient profiles of the lncRNAs. Each curve corresponds to an individual lncRNA. (d) Venn diagram showing the mRNAs co-expressed with the five lncRNAs in the TCGA cohort (Pearson correlation coefficient > 0.1). (e-f) KEGG pathway (e) and GO term (f) enrichment analyses of mRNAs co-expressed with the five lncRNAs. Abbreviations: pRFS, peritoneal recurrence-free survival; SYSUCC, Sun Yat-sen University Cancer Center; HR, hazard ratio; CI, confidence interval.

LASSO regression modeling was applied to select five lncRNAs (CASC15, CH17-360D5.2, LINC01094, MIR4435-2HG, and RP11-400N13.3) as candidate predictors of peritoneal metastasis **(Figures 2b and 2c)**. Analysis of the TCGA dataset revealed 610 mRNAs that exhibited strong co-expression relationships with these five lncRNAs **(Figure 2d)**. Enrichment analyses demonstrated that the co-expressed mRNAs were significantly overrepresented in multiple critical cancer-associated pathways and biological processes, including the PI3K-Akt signaling pathway, ECM-receptor interaction, focal adhesion, and collagen-containing extracellular matrix **(Figures 2e and 2f)**. These pathways play established roles in driving cancer metastasis [17] and modulating the composition of the extracellular matrix at metastatic sites [18]. These findings emphasize their mechanistic importance in GC peritoneal metastasis and support their relevance for predicting peritoneal recurrence.

Construction of a PM risk score for forecasting peritoneal recurrence in gastric cancer

In the discovery stage, a PM risk score was formulated by integrating the expression of the five candidate lncRNAs to estimate the likelihood of peritoneal recurrence. During validation, the calculated PM risk score and associated clinicopathological variables for the 231 patients comprising the SYSUCC cohort are displayed in **Figure 3a**. Patients with peritoneal metastasis showed notably elevated PM risk scores. Based on this score, the cohort was divided into a high-risk group of 149 patients and a low-risk group of 82 patients. Survival analyses using the Kaplan-Meier method indicated that patients assigned to the high PM risk score category had significantly inferior pRFS **(Figure 3b)**, RFS **(Figure 3c)**, and OS **(Figure 3d)**. The corresponding hazard ratios were 2.04 (95% confidence

interval [CI]: 1.35–3.07; P < 0.001), 1.93 (95% CI: 1.31–2.85; P < 0.001), and 1.83 (95% CI: 1.21–2.76; P = 0.004), respectively. Additionally, the high-risk group demonstrated markedly higher rates of peritoneal recurrence and overall mortality than the low-risk group **(Figure 3e)**. In the TCGA dataset, where peritoneal recurrence information was unavailable, the prognostic value of the PM risk score was evaluated based on overall survival. The PM risk score distribution and clinicopathological parameters for the 414 patients are illustrated in **Figure 3f**. Kaplan-Meier curves revealed shorter OS among patients with high PM risk scores **(Figure 3g)**, with a hazard ratio of 1.82 (high versus low; 95% CI: 1.23–2.68; P = 0.003). These outcomes closely aligned with those observed in the SYSUCC cohort, confirming the PM risk score's effectiveness for prognostic stratification in GC.

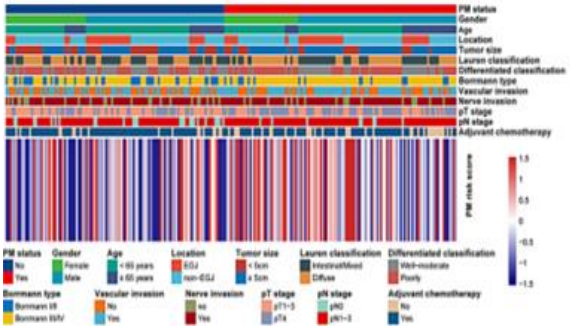

a)

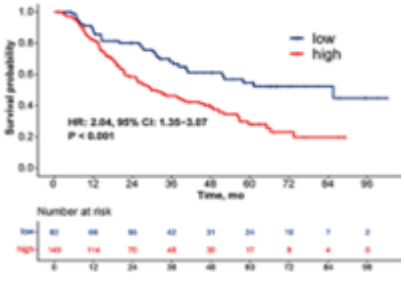

b)

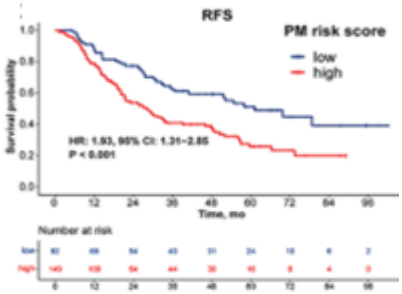

c)

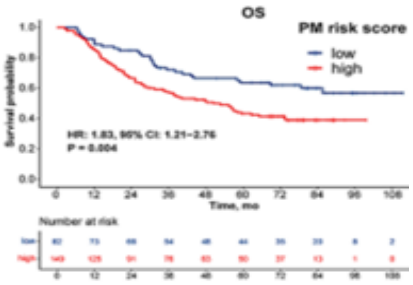

d)

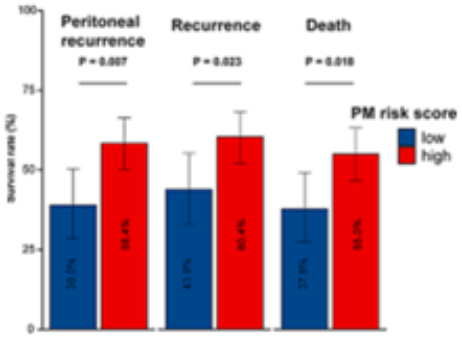

e)

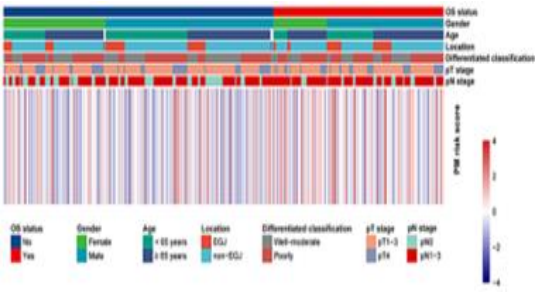

f)

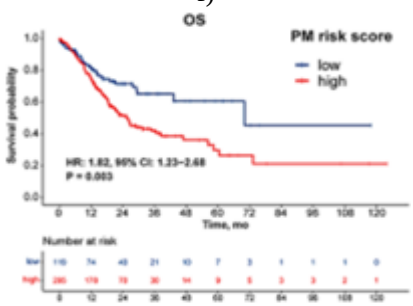

g)

Figure 3. Construction of a PM Risk Score for Forecasting Peritoneal Recurrence in Gastric Cancer

(a) Heatmap showing the distribution of the PM risk score, along with relevant clinicopathologic features, in the SYSUCC validation cohort, (b-d) Kaplan-Meier curves showing the probability of pRFS (b), RFS (c), and OS (d) for patients stratified by high and low PM risk scores, (E) Boxplot comparing the incidence of peritoneal recurrence, overall recurrence, and mortality

between patients with high and low PM risk scores, (f) Heatmap showing the distribution of the PM risk score and corresponding clinicopathologic characteristics in the TCGA cohort, and (g) Kaplan-Meier curves illustrating OS probability for patients with high versus low PM risk scores. Abbreviations: SYSUCC, Sun Yat-sen University Cancer Center; TCGA, The Cancer Genome Atlas; PM, peritoneal metastasis; EGJ, esophagogastric junction; pRFS, peritoneal recurrence-free survival; RFS, recurrence-free survival; OS, overall survival; HR, hazard ratio; CI, confidence interval

Integrated score enhances model performance in predicting peritoneal Recurrence among gastric cancer patients

Univariate and multivariate Cox regression models were applied to assess associations with pRFS, RFS, and OS within the SYSUCC cohort. **Table 1** indicates that the PM risk score, tumor diameter, pT category, pN category, and adjuvant chemotherapy were independent prognostic factors for pRFS. To augment the predictive capability of the PM risk score, it was combined with tumor size, pT stage, and pN stage to generate a competing-risks nomogram **(Figure 4a)**. This combined model achieved robust discrimination for pRFS, yielding a 5-year AUC of 0.79 (95% CI: 0.71−0.88) **(Figure 4b)**. Integrated scores derived from the nomogram enabled reclassification of SYSUCC cohort patients into high-risk (n = 157) and low-risk (n = 74) subgroups. Survival disparities between these subgroups were substantially larger than those obtained using the PM risk score alone (pRFS: hazard ratio [HR] 4.57, 95% CI: 2.72–7.66, $P < 0.001$; RFS: HR 3.81, 95% CI: 2.38–6.10, $P < 0.001$; OS: HR 4.50, 95% CI: 2.64–7.65, $P < 0.001$) **(Figure 4c)**. Moreover, the integrated score demonstrated superior predictive accuracy for pRFS, RFS, and OS at the 2-, 3-, and 5-year time points relative to the other individual clinicopathological factors ($P < 0.05$), **(Figure 4D)**.

Table 1. Uni- and multivariable Cox regression of pRFS, RFS and OS in the SYSUCC cohort.

Outcome	Variable	P-value	Multivariable HR (95% CI)	P-value	Univariable HR (95% CI)
pRFS	PM risk score (high vs. low)	0.011	1.73 (1.14–2.64)	< 0.001	2.04 (1.35–3.07)
	Sex (male vs. female)	—	—	0.153	1.33 (0.90–1.95)
	Age group (≥ 65 vs. < 65 years)	—	—	0.509	1.14 (0.77–1.70)
	Tumor location (non-EGJ vs. EGJ)	—	—	0.882	0.97 (0.67–1.41)
	Tumor diameter (≥ 5 vs. < 5 cm)	0.008	1.87 (1.18–2.95)	< 0.001	2.53 (1.64–3.90)
	Borrmann classification (III–IV vs. I–II)	0.086	1.60 (0.93–2.75)	< 0.001	2.65 (1.60–4.38)
	Histological differentiation (G3 vs. G1/G2)	—	—	0.453	1.15 (0.80–1.66)
	Lauren subtype (Diffuse vs. Intestinal/mixed)	—	—	0.672	1.08 (0.75–1.55)
	Perineural invasion (present vs. absent)	—	—	0.135	1.47 (0.89–2.42)
	Lymphovascular invasion (present vs. absent)	0.377	1.18 (0.81–1.72)	0.025	1.52 (1.05–2.19)
	Pathological T stage (T4 vs. T1–3)	0.045	1.49 (1.01–2.21)	< 0.001	2.16 (1.49–3.13)
	Pathological N stage (N1–3 vs. N0)	0.005	2.90 (1.39–6.05)	0.003	2.98 (1.45–6.11)
	Adjuvant chemotherapy (received vs. not received)	0.003	0.55 (0.37–0.82)	0.001	0.53 (0.36–0.78)
RFS	PM risk score (high vs. low)	0.014	1.66 (1.11–2.47)	< 0.001	1.93 (1.31–2.85)
	Sex (male vs. female)	—	—	0.072	1.42 (0.97–2.07)
	Age group (≥ 65 vs. < 65 years)	—	—	0.344	1.20 (0.82–1.75)
	Tumor location (non-EGJ vs. EGJ)	—	—	0.989	1.00 (0.70–1.44)
	Tumor diameter (≥ 5 vs. < 5 cm)	0.005	1.90 (1.21–2.97)	< 0.001	2.57 (1.68–3.92)
	Borrmann classification (III–IV vs. I–II)	0.123	1.49 (0.90–2.46)	< 0.001	2.40 (1.50–3.84)
	Histological differentiation (G3 vs. G1/G2)	—	—	0.679	1.08 (0.76–1.54)
	Lauren subtype (Diffuse vs. Intestinal/mixed)	—	—	0.985	1.00 (0.70–1.42)
	Perineural invasion (present vs. absent)	—	—	0.217	1.35 (0.84–2.18)
	Lymphovascular invasion (present vs. absent)	0.270	1.23 (0.85–1.77)	0.021	1.52 (1.07–2.17)
	Pathological T stage (T4 vs. T1–3)	0.039	1.49 (1.02–2.18)	< 0.001	2.10 (1.46–3.00)
	Pathological N stage (N1–3 vs. N0)	0.019	2.14 (1.13–4.05)	0.010	2.25 (1.21–4.18)
	Adjuvant chemotherapy (received vs. not received)	0.008	0.58 (0.40–0.87)	0.003	0.55 (0.38–0.81)

OS	PM risk score (high vs. low)	0.037	1.57 (1.03–2.41)	0.004	1.83 (1.21–2.76)
	Sex (male vs. female)	—	—	0.255	1.26 (0.85–1.87)
	Age group (≥ 65 vs. < 65 years)	—	—	0.318	1.23 (0.82–1.84)
	Tumor location (non-EGJ vs. EGJ)	—	—	0.624	0.91 (0.62–1.33)
	Tumor diameter (≥ 5 vs. < 5 cm)	0.009	1.89 (1.17–3.05)	< 0.001	2.55 (1.63–3.97)
	Borrmann classification (III–IV vs. I–II)	0.158	1.49 (0.86–2.60)	< 0.001	2.51 (1.49–4.20)
	Histological differentiation (G3 vs. G1/G2)	—	—	0.470	1.15 (0.79–1.66)
	Lauren subtype (Diffuse vs. Intestinal/mixed)	—	—	0.467	1.15 (0.79–1.66)
	Perineural invasion (present vs. absent)	—	—	0.109	1.54 (0.91–2.62)
	Lymphovascular invasion (present vs. absent)	0.188	1.29 (0.88–1.89)	0.013	1.61 (1.10–2.34)
	Pathological T stage (T4 vs. T1–3)	0.131	1.36 (0.91–2.04)	< 0.001	2.01 (1.38–2.93)
	Pathological N stage (N1–3 vs. N0)	0.006	2.80 (1.33–5.87)	0.002	3.08 (1.50–6.33)
	Adjuvant chemotherapy (received vs. not received)	< 0.001	0.45 (0.30–0.67)	< 0.001	0.46 (0.31–0.69)

Abbreviations: SYSUCC, Sun Yat-Sen University Cancer Center; pRFS, peritoneal recurrence-free survival; RFS, recurrence-free survival; OS, overall survival; HR, hazard ratio; CI, confidence interval; PM, peritoneal metastasis; EGJ, esophagogastric junction.

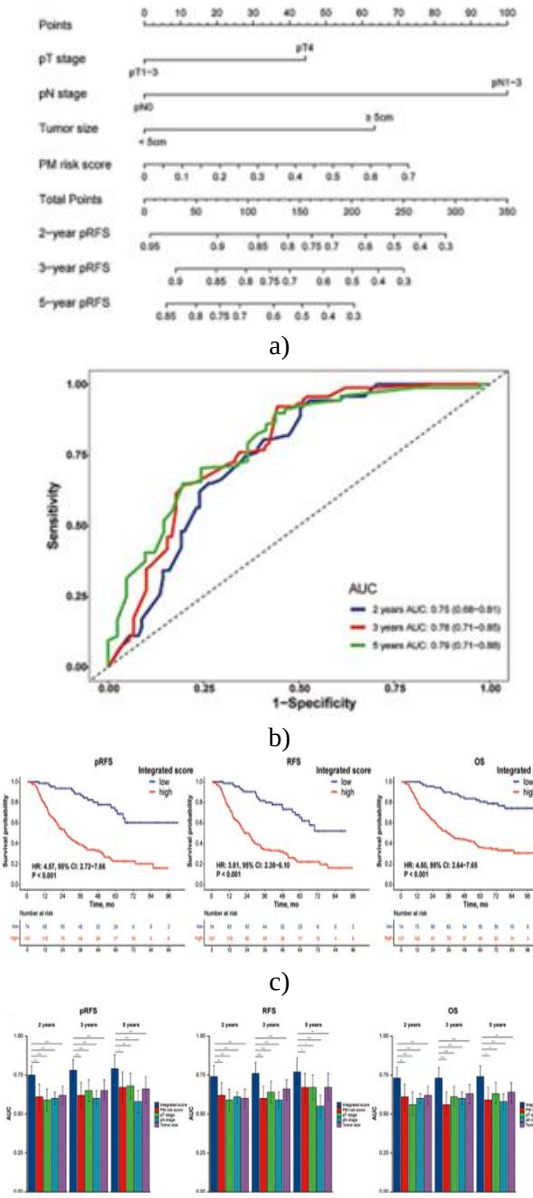

Figure 4. Integrated Score Enhances Model Performance in Predicting Peritoneal Recurrence

(a) Nomogram constructed via Cox regression that incorporates the PM risk score, pathological T and N stages, and tumor size within the SYSUCC validation cohort, (b) Time-dependent receiver operating characteristic (ROC) curves evaluating 2-, 3-, and 5-year pRFS predictions based on the integrated score, (c) Kaplan-Meier curves showing the probability of pRFS (left panel), RFS (middle panel), and OS (right panel) for patients with high and low integrated scores, and (d) Boxplot contrasting the AUC values of the integrated score with those of the remaining variables. *P < 0.05, **P < 0.01, ***P < 0.001, ****P < 0.0001. Abbreviations: PM, peritoneal metastasis; pRFS, peritoneal recurrence-free survival; RFS, recurrence-free survival; OS, overall survival; HR, hazard ratio; CI, confidence interval; AUC, area under the curve.

Subgroup evaluation according to integrated score level revealed that patients in the high-score category within the SYSUCC cohort experienced significant clinical benefit from adjuvant chemotherapy, manifested as prolonged pRFS (HR: 0.52, 95% CI: 0.34–0.79, P = 0.002), RFS (HR: 0.53, 95% CI: 0.35–0.80, P = 0.003), and OS (HR: 0.40, 95% CI: 0.26–0.62, P < 0.001). Conversely, individuals in the low-score category showed no meaningful improvement in pRFS, RFS, or OS with adjuvant chemotherapy.

An analogous integrated score was established in the TCGA cohort by merging the PM risk score with age and pN stage following the same methodology. This score

effectively stratified patient survival (5-year OS AUC: 0.79, 95% CI: 0.71–0.88), although its overall discriminatory capacity was modestly lower than that observed in the SYSUCC cohort.

CASC15 drives metastatic potential of gastric cancer cells both in vitro and in vivo

To explore the biological functions underlying the predictive value of lncRNAs for peritoneal metastasis and patient survival, the focus was on transcripts with the strongest hazard ratios. RP11-426C22.4 and CTD-2227E11.1 were excluded from further study because survival analyses revealed no statistically significant associations. Of the remaining candidates, CASC15 was prioritized over RP11-400N13.3 due to its higher contribution coefficient in the LASSO regression analysis. Expression profiling by quantitative RT-PCR demonstrated varying levels of CASC15 across gastric cancer cell lines and the non-transformed GES-1 gastric epithelial cells. Stable cell lines with CASC15 knockdown or overexpression were successfully engineered and verified in GC cells. Functional experiments, including wound-healing assays, Transwell migration and invasion assays, and 3D tumor spheroid invasion models, consistently indicated that reducing CASC15 expression substantially attenuated the migratory and invasive phenotypes of GC cells **(Figures 5a-5e)**; (all $P < 0.05$).

In contrast, ectopic expression of CASC15 markedly enhanced cell migration and invasion **(Figures 5f-5h)**; (all $P < 0.05$). Complementary CCK-8 and colony formation assays further showed that CASC15 influenced cell proliferative ability. Of note, silencing CASC15 significantly increased cellular sensitivity to the first-line gastric cancer chemotherapeutic agents 5-FU and oxaliplatin. This finding is consistent with the clinical observation that patients with high integrated scores in the SYSUCC cohort experienced therapeutic benefit from adjuvant chemotherapy.

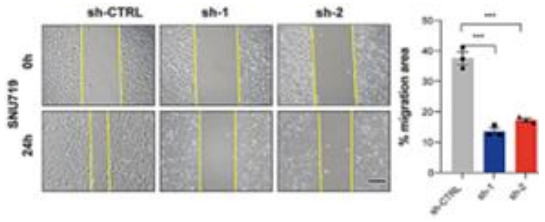

a)

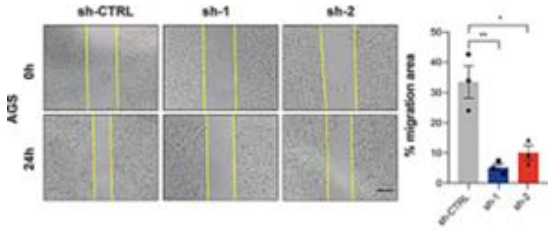

b)

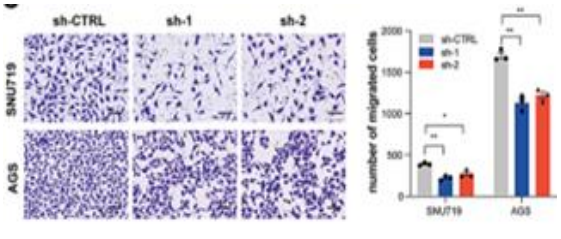

c)

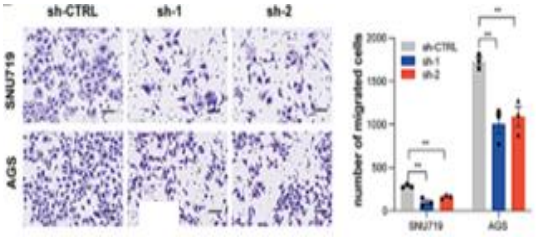

d)

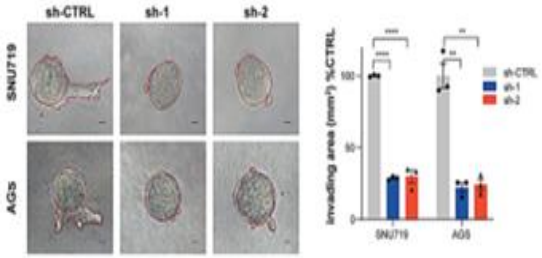

e)

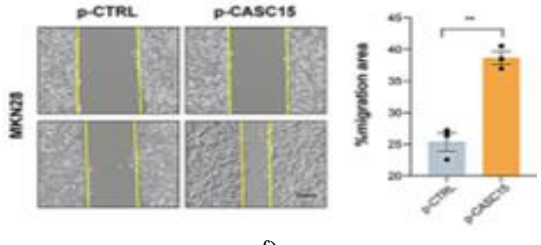

f)

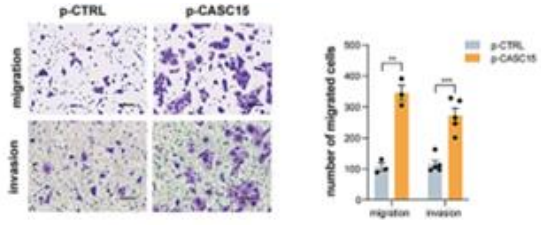

g)

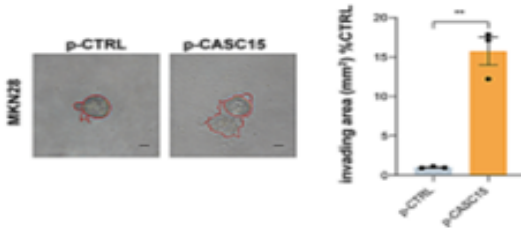

h)

Figure 5. Source data are provided in the Source Data file.

*P < 0.05, **P < 0.01, ***P < 0.001, ****P < 0.0001

CASC15 Promotes Metastasis of GC Cells In Vitro: (a-b) Wound-healing assay evaluating the consequences of CASC15 depletion on the migratory properties of the specified GC cell lines. Left panels: representative photomicrographs. Right panels: bar graphs quantifying the percentage of wound closure. Scale bar, 200 μm. (c-d) Transwell assay assessing the influence of CASC15 knockdown on migratory (c) and invasive (d) capacities of the indicated GC cells. Left panels: representative images. Scale bar, 100 μm. Right panels: bar graphs showing the counts of migrated or invaded cells. (e) 3D multicellular tumor spheroid invasion assay examining the impact of CASC15 silencing on the invasive behavior of the indicated GC cells. Left panels: representative images. Scale bar, 20 μm. Right panel: quantification of the invading area relative to the spheroid core, normalized to control conditions. (f) Wound-healing assay determining the effects of CASC15 overexpression on cell migration in the specified GC cell lines. Left panels: representative photomicrographs. Right panel: bar graph depicting the percentage of wound closure area. Scale bar, 200 μm. (g) Transwell assay investigating the impact of CASC15 overexpression on migration (upper panels) and invasion (lower panels) in the indicated GC cells. Left panels: representative images. Scale bar, 100 μm. Right panels: bar graphs presenting the numbers of migrated and invaded cells, and (h) 3D multicellular tumor spheroid invasion assay analyzing the influence of CASC15 overexpression on invasive capacity of the indicated GC cells. Left panels: representative images. Scale bar, 20 μm. Right panel: bar graph illustrating the ratio of invading area to spheroid body, normalized to the control group. The red line highlights the boundary between the spheroid core and the invading region. For (a-h), results are expressed as mean ± SEM, with individual data points from separate experiments displayed as dots. Statistical comparisons were conducted using a two-tailed unpaired Student's t-test.

To determine whether CASC15 enhances peritoneal metastasis (PM) of gastric cancer (GC) in living organisms, we generated a xenograft mouse model by injecting GC cells into the peritoneal cavity of Balb/c nude mice and NOG mice. Continuous monitoring was performed using an in vivo small-animal fluorescence imaging system (IVIS). IVIS imaging showed a substantial decrease in the ability of GC cells to form tumors in the peritoneal cavity when CASC15 was silenced, in contrast to the control group; the reverse pattern emerged upon CASC15 overexpression **(Figures 6a-6e)**, (P < 0.05). After 3 or 4 weeks, the mice were euthanized, and abdominal tumor counts were performed, confirming the same outcome (P < 0.05).

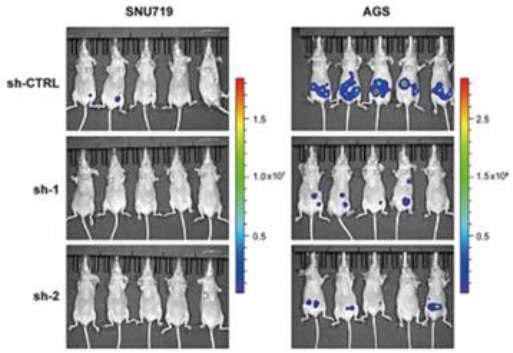

a)

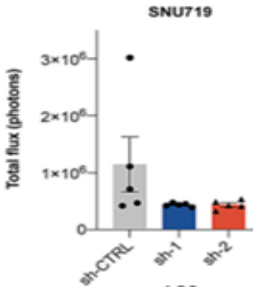

b)

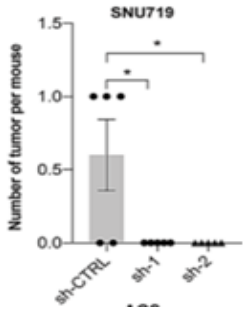

c)

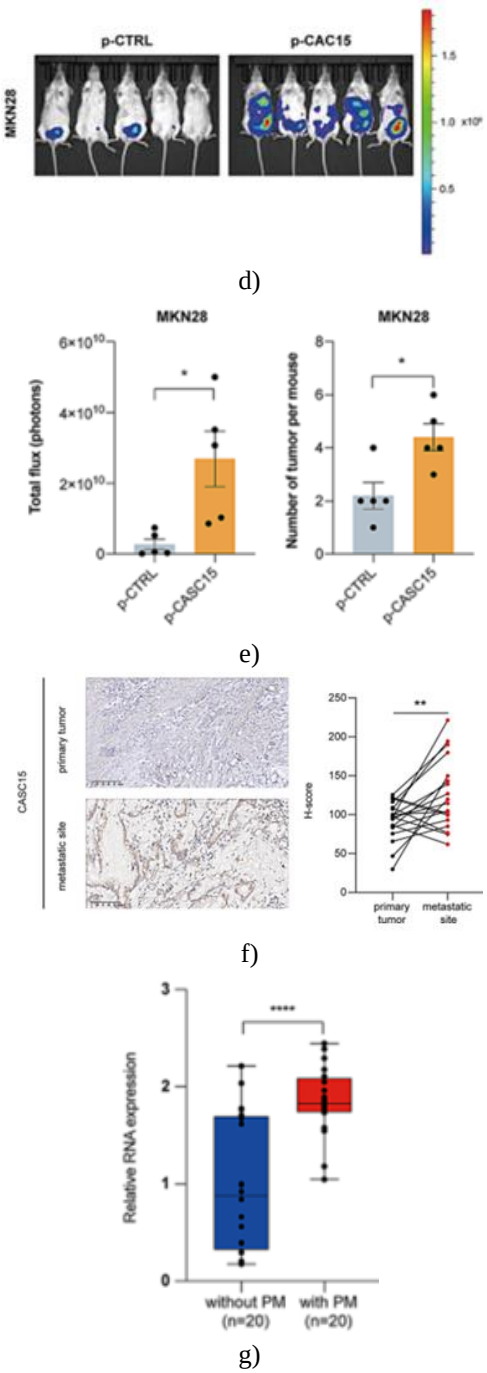

Figure 6. Source data are provided in the Source Data file.

*P < 0.05, **P < 0.01, ***P < 0.001, ****P < 0.0001, ns, no significance. CASC15 promotes peritoneal metastasis of GC cells in vivo: (a-c) IVIS assay showing the consequences of CASC15 knockdown on tumorigenic potential in the designated GC cell lines (n = 5 mice). (a) Representative bioluminescence images from each experimental group at 3 or 4 weeks, (b) Histograms illustrating photon luminescent intensity, (c) Histograms presenting the number of tumors per mouse. Tumor numbers were established by counting xenografts recovered from the abdominal cavity post-dissection, (d-e) IVIS assay illustrating the consequences of CASC15 overexpression on tumorigenic potential in the designated GC cell lines (n = 5 mice). (d) Representative bioluminescence images from each experimental group at 4 weeks; (e) Histogram of photon luminescent intensity (left) and histogram of tumor numbers per mouse (right). Tumor numbers were established by counting xenografts recovered from the abdominal cavity post-dissection. (f) CASC15 expression was examined by in situ hybridization in primary tumors and metastatic lesions from patients with peritoneal metastases of gastric cancer. Left: representative images. Scale bar, 100 μm. Right: Chart of H-score. (g) Boxplot showing relative CASC15 abundance in plasma of patients with or without peritoneal metastases. For (a-e), data represent mean ± SEM; the dot plot reflects data points from each mouse. Statistical analysis was conducted using a two-tailed unpaired Student's t-test. For (F), the dot plot reflects data points from each patient and the lines represent paired tissues. Statistical analysis was conducted using a paired t-test. For (G), the data range from min to max; the dot plot shows data points from each patient. Statistical analysis was conducted using a Wilcoxon test.

Subsequently, we procured GC tissue samples from 19 patients with PM, including matched primary gastric tumors and peritoneal metastatic specimens, and assessed CASC15 expression levels by in situ hybridization. Consistent with the experimental data, CASC15 showed markedly higher expression in metastatic lesions than in corresponding primary tumors, reinforcing its role in driving gastric cancer metastasis **(Figure 6f)**. Furthermore, plasma CASC15 concentrations were analyzed in 40 patients, revealing significantly elevated levels in patients with PM. These findings support the potential of CASC15 as a biomarker for predicting peritoneal metastasis risk **(Figure 6g)**, (P < 0.05).

CASC15 promotes the metastasis of GC via the p38 and JNK signaling pathways

To investigate the molecular basis by which CASC15 drives gastric cancer (GC) metastasis, we initially assessed the subcellular distribution of CASC15 in GC cells, revealing predominant cytoplasmic localization

(Figure 7a). We then performed RNA sequencing in SNU719 cells stably depleted of CASC15 compared with control cells. KEGG and GO enrichment analyses of genes downregulated upon CASC15 silencing identified strong associations with epithelial-mesenchymal transition (EMT)-related processes, encompassing extracellular matrix organization, extracellular structure organization, wound healing, cell-substrate junction assembly, and focal adhesion **(Figure 7b)**. In agreement with this, expression of N-cadherin, Vimentin, and α-smooth muscle actin decreased markedly, while E-cadherin and β-catenin increased after CASC15 depletion. Reciprocal changes occurred in cells overexpressing CASC15 **(Figures 7c and 7d)**. Transcriptional shifts in these EMT markers mirrored the alterations at the protein level, implying that CASC15 primarily controls their abundance through transcriptional regulation. Moreover, depletion of CASC15 reduced pseudopodia formation, whereas its enforced expression increased it. Together, these observations indicate that CASC15 facilitates GC cell metastasis by enhancing EMT.

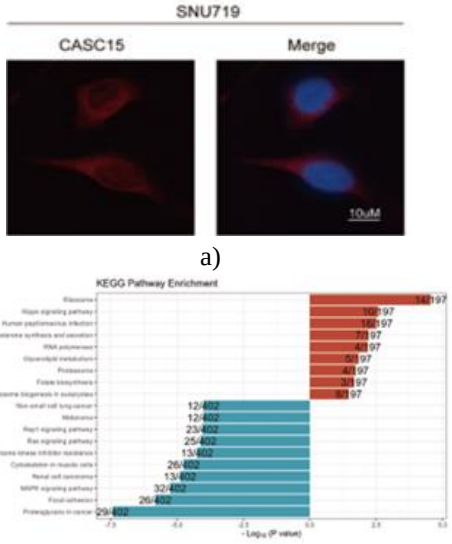

a)

b)

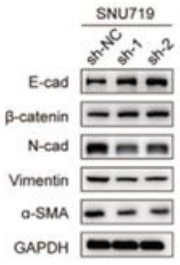

c)

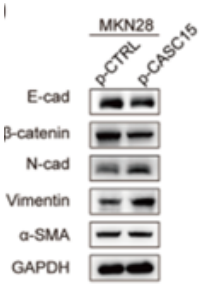

d)

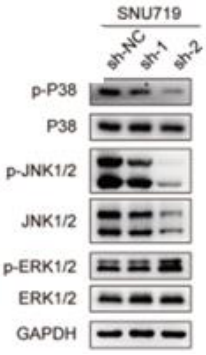

e)

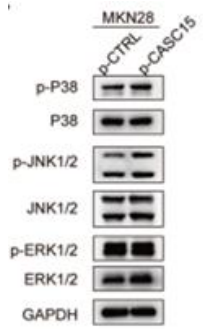

f)

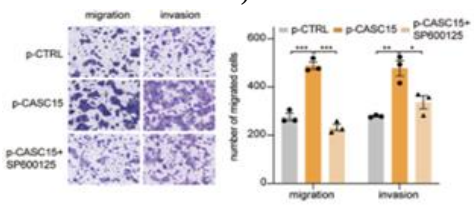

g)

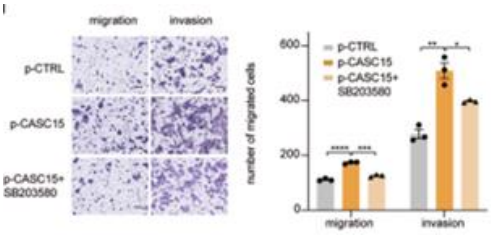

h)

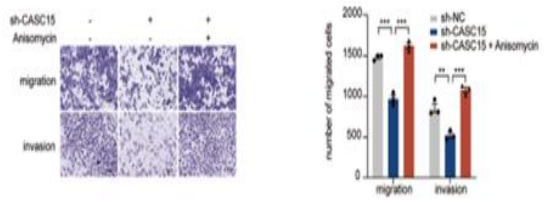

i)

Figure 7. Source data are provided in the Source Data file. *P < 0.05, **P < 0.01, ***P < 0.001, ****P < 0.0001. CASC15 promotes the metastasis of GC via the p38 and JNK signaling pathways

(a) RNA immuno-FISH analysis illustrating the intracellular distribution of CASC15 in GC cells, (b) KEGG pathway enrichment analysis of differentially expressed mRNAs in CASC15-knockdown GC cells versus control cells, (c-d) Western blot results depicting the influence of CASC15 knockdown (c) and overexpression (d) on protein levels of major epithelial-mesenchymal transition (EMT) regulators. (e-f) Western blot results depicting the influence of CASC15 knockdown (e) and overexpression (f) on protein levels of major components in the MAPK signaling cascade. (g-h) Transwell assay indicating that SP600125 (20 μM for 24 h) and SB203580 (15 μM for 24 h) abrogate the enhancement of GC cell migration and invasion induced by CASC15 overexpression. Left: representative images. Scale bar, 100 μm. Right: Quantification of migratory and invasive cell numbers, and (i) Transwell assay indicating that anisomycin (100 nM for 12 h) abrogates the suppression of GC cell migration and invasion caused by CASC15 knockdown. Left: representative images. Scale bar, 100 μm. Right: Quantification of migratory and invasive cell numbers. For (g-i), data represent mean ± SEM from three independent experiments; the dot plot reflects data points from independent experiments. Statistical analysis was performed using a two-tailed unpaired Student's t-test.

Enrichment analysis of genes suppressed in CASC15-knockdown cells prominently implicated the MAPK signaling pathway. We subsequently explored whether MAPK signaling accounts for CASC15 function and detected pronounced reductions in phosphorylated JNK and p38 upon CASC15 depletion, with reciprocal elevations in overexpressing cells **(Figures 7e and 7f)**. To clarify the relevance of p38 and JNK branches of MAPK signaling in CASC15-associated GC progression, rescue studies were performed employing the JNK inhibitor SP600125 and the p38 inhibitor SB203580. Both compounds effectively diminished the elevated migration and invasion abilities resulting from CASC15 overexpression **(Figures 7g and 7h)**. Notably, application of anisomycin, a dual JNK/p38 activator, successfully reinstated migratory and invasive properties in CASC15-depleted GC cells **(Figure 7i)**. These results establish that CASC15 exerts its pro-metastatic effects in GC through reliance on JNK and p38 signaling pathways.

Long non-coding RNAs (lncRNAs) serve as important biomarkers, exhibiting characteristic expression signatures across diverse physiological and disease states that provide essential information for diagnostic and prognostic purposes [19]. Their frequent tissue- and disease-specific patterns support highly selective and accurate identification of pathological conditions [20]. In addition, the stability of lncRNAs and their detectability across various biological specimens increase their value for clinical biomarker applications and targeted treatment strategies [21]. The current investigation examined the usefulness of lncRNAs for identifying peritoneal metastasis (PM) in gastric cancer (GC). Comprehensive lncRNA transcriptome analysis was conducted on matched peritoneal metastatic lesions, primary gastric tumors, and adjacent normal tissues collected from 12 GC patients within the SYSUCC discovery set. By integrating these data with the TCGA database, 10 pivotal lncRNAs were selected. Five promising candidates were further refined through cross-validation and least absolute shrinkage and selection operator (LASSO) regression using the SYSUCC validation cohort. From this information, a PM risk score was formulated to estimate peritoneal recurrence-free survival (pRFS), with higher scores indicating a greater risk of peritoneal relapse. An integrated nomogram was then constructed by combining the PM risk score with pT stage, pN stage, and tumor diameter. This composite model demonstrated robust forecasting capability for pRFS, recurrence-free survival (RFS), and overall survival (OS) among GC patients who underwent radical gastrectomy, while also improving patient selection for adjuvant chemotherapy. Detailed functional analyses of the prominent lncRNA CASC15 revealed its strong capacity to stimulate GC cell metastatic behavior in vitro and to drive PM formation in vivo. Mechanistic exploration further showed that CASC15 induces epithelial-mesenchymal transition (EMT) by activating the JNK and p38 branches of the MAPK pathway, thereby promoting gastric cancer metastasis.

Collectively, these findings supply foundational support for the participation of lncRNAs in GC peritoneal dissemination. To promote translational relevance, an lncRNA-derived integrated scoring system was established to forecast peritoneal recurrence risk at the individual level. In parallel, circulating CASC15 emerged as a potential noninvasive indicator for PM detection in GC.

Peritoneal metastasis constitutes a major therapeutic obstacle and is the leading cause of recurrence following radical resection in GC cases [2, 5, 22]. Despite this, sensitive and specific tools for diagnosing postoperative peritoneal relapse are still insufficient, primarily because of postsurgical modifications in abdominal anatomy that impede accurate assessment. Conventional radiological approaches also face notable constraints. Previous efforts to tackle this issue include the transcriptomic signature developed by Lee *et al*. [23] for stratifying risk of peritoneal carcinomatosis, the miRNA signature proposed by Shimura *et al*. [24] for PM detection in GC, and the collagen-based nomogram introduced by Chen *et al*. [25] for PM risk evaluation in serosa-invading GC after curative resection. Nonetheless, widespread clinical implementation of these models has not yet been realized. The present work adopted a distinct whole-transcriptome lncRNA approach. It merged it with standard clinicopathological parameters to generate a multifaceted predictive score capable of anticipating not only peritoneal recurrence but also broader recurrence and survival outcomes. This broader utility likely stems from the fact that peritoneal spread is the dominant mode of recurrence and a key contributor to mortality in GC.

Diagnosis of PM that coincides with primary GC detection or occurs during planned curative surgery is known as synchronous PM. In contrast, peritoneal relapse manifesting after successful radical gastrectomy is termed metachronous PM. This study primarily examined synchronous PM specimens to delineate the lncRNA transcriptional profile and uncover key regulatory transcripts. The rationale included the feasibility of obtaining matched primary tumor, metastatic, and normal mucosal samples from the same patient, as well as the absence of prior therapeutic exposure, which enhances data integrity. Supporting this strategy, Chen *et al*. [26] reported common molecular alterations in synchronous and metachronous PM, suggesting potentially overlapping pathogenic processes. Consequently, the risk model derived from synchronous cases performed well at predicting metachronous peritoneal recurrence. A noteworthy additional finding was an elevated plasma CASC15 concentration in patients with PM compared with those without. Taken together, these data highlight CASC15 as a promising marker for both synchronous and metachronous forms of PM, suggesting considerable potential for future clinical use.

Adjuvant chemotherapy is routinely recommended for patients diagnosed with pathological stages II and III [7, 27]. However, not all patients derive equal benefits from adjuvant chemotherapy [28], particularly those with mismatch repair deficiency (dMMR)/microsatellite instability-high (MSI-H) [29], and such patients may require more precise stratification to avoid chemotherapy-related adverse effects and unnecessary financial burdens.

Our findings indicated that individuals with high integrated scores gained considerable therapeutic benefit from adjuvant chemotherapy, whereas those with low scores did not show a meaningful improvement in clinical outcomes. In addition, reducing CASC15 expression heightened the susceptibility of gastric cancer cells to conventional first-line agents, notably 5-FU and oxaliplatin. These results suggest that the integrated score could serve as a practical tool for postoperative risk assessment in GC, while interventions targeting CASC15 suppression might enhance chemosensitivity. Nonetheless, given the modest cohort size, potential selection biases cannot be dismissed, necessitating confirmation in future large-scale prospective trials.

From a conceptual standpoint, lncRNAs are well positioned to predict peritoneal metastasis (PM) in GC owing to their central role in regulating metastatic cascades. Prior reports have documented that lncRNAs may either augment or restrain PM development in GC by influencing mechanisms including ferroptosis [30] and alterations in fatty acid metabolism [31]. Within this investigation, CASC15 was prioritized for in-depth characterization. Experimental data confirmed that varying CASC15 levels directly affected GC cell motility and invasiveness in vitro, as well as their ability to establish peritoneal metastases in vivo. The metastatic-promoting function of CASC15 operates principally through the JNK and p38 MAPK signaling axes. These insights furnish mechanistic grounding for the application of lncRNAs in PM risk prediction for gastric cancer.

This study is subject to certain constraints. Chief among them is the lack of comprehensive recurrence timing and

pattern data in the TCGA repository, which precluded independent external validation of the developed score. While our analyses support the efficacy of the lncRNA-derived model in anticipating both synchronous and metachronous peritoneal spread in gastric cancer, multicenter validation studies are required to substantiate its generalizability. Another consideration is the reliance on invasively acquired tumor tissue for score computation. On a positive note, our work underscores the viability of plasma CASC15 measurement as a minimally invasive liquid biopsy approach for assessing peritoneal metastasis risk in GC. Subsequent research endeavors will focus on larger patient populations to further corroborate this biomarker's clinical value.

Conclusion

In summary, the current investigation mapped the lncRNA expression landscape in gastric cancer. It developed an integrated lncRNA-based scoring system that facilitates personalized forecasts of peritoneal recurrence and patient survival in routine practice. Importantly, this composite metric reliably distinguishes patients most likely to benefit from adjuvant chemotherapy, thereby aiding the refinement of individualized treatment plans.

Acknowledgments: None

Conflict of Interest: None

Financial Support: None

Ethics Statement: None

References

1. Sung H, Ferlay J, Siegel RL, Laversanne M, Soerjomataram I, Jemal A, et al. Global Cancer statistics 2020: GLOBOCAN estimates of incidence and Mortality Worldwide for 36 cancers in 185 countries. CA Cancer J Clin. 2021;71(3):209–49.
2. Yoo CH, Noh SH, Shin DW, Choi SH, Min JS. Recurrence following curative resection for gastric carcinoma. Br J Surg. 2000;87(2):236–42.
3. Sasako M, Sano T, Yamamoto S, Kurokawa Y, Nashimoto A, Kurita A, et al. D2 lymphadenectomy alone or with para-aortic nodal dissection for gastric cancer. N Engl J Med. 2008;359(5):453–62.
4. Fujitani K, Yang HK, Mizusawa J, Kim YW, Terashima M, Han SU, et al. Gastrectomy plus chemotherapy versus chemotherapy alone for advanced gastric cancer with a single non-curable factor (REGATTA): a phase 3, randomised controlled trial. Lancet Oncol. 2016;17(3):309–18.
5. Thomassen I, van Gestel YR, van Ramshorst B, Luyer MD, Bosscha K, Nienhuijs SW, et al. Peritoneal carcinomatosis of gastric origin: a population-based study on incidence, survival and risk factors. Int J Cancer. 2014;134(3):622–8.
6. Burbidge S, Mahady K, Naik K. The role of CT and staging laparoscopy in the staging of gastric cancer. Clin Radiol. 2013;68(3):251–5.
7. Wang FH, Zhang XT, Tang L, Wu Q, Cai MY, Li YF, et al. The Chinese Society of Clinical Oncology (CSCO): clinical guidelines for the diagnosis and treatment of gastric cancer, 2023. Cancer Commun (Lond). 2024;44(1):127–72.
8. Dong D, Tang L, Li ZY, Fang MJ, Gao JB, Shan XH, et al. Development and validation of an individualized nomogram to identify occult peritoneal metastasis in patients with advanced gastric cancer. Ann Oncol. 2019;30(3):431–8.
9. Kim SJ, Kim HH, Kim YH, Hwang SH, Lee HS, Park do J, et al. Peritoneal metastasis: detection with 16- or 64-detector row CT in patients undergoing surgery for gastric cancer. Radiology. 2009;253(2):407–15.
10. Mattick JS, Amaral PP, Carninci P, Carpenter S, Chang HY, Chen LL, et al. Long non-coding RNAs: definitions, functions, challenges and recommendations. Nat Rev Mol Cell Biol. 2023;24(6):430–47.
11. Statello L, Guo CJ, Chen LL, Huarte M. Gene regulation by long non-coding RNAs and its biological functions. Nat Rev Mol Cell Biol. 2021;22(2):96–118.
12. Ali SA, Peffers MJ, Ormseth MJ, Jurisica I, Kapoor M. The non-coding RNA interactome in joint health and disease. Nat Rev Rheumatol. 2021;17(11):692–705.
13. Zhou M, Bao S, Gong T, Li Q, Xie J, Li X, et al. The transcriptional landscape and diagnostic potential of long non-coding RNAs in esophageal squamous cell carcinoma. Nat Commun. 2023;14(1):3799.
14. Dong C, Luan F, Tian W, Wang M, Zhang J, Liu X, et al. Identification and validation of crucial lnc-

TRIM28-14 and hub genes promoting gastric cancer peritoneal metastasis. BMC Cancer. 2023;23(1):76.
15. Wang S, Wo L, Zhang Z, Kang Y, Peng Q, Li Z, et al. Delivery of LINC00589 via mesoporous silica nanoparticles inhibits peritoneal metastasis in gastric cancer. Cancer Lett. 2022;549:215916.
16. Chen RX, Chen X, Xia LP, Zhang JX, Pan ZZ, Ma XD, et al. N6-methyladenosine modification of circNSUN2 facilitates cytoplasmic export and stabilizes HMGA2 to promote colorectal liver metastasis. Nat Commun. 2019;10(1):4695.
17. He Y, Sun MM, Zhang GG, Yang J, Chen KS, Xu WW, et al. Targeting PI3K/Akt signal transduction for cancer therapy. Signal Transduct Target Ther. 2021;6(1):425.
18. Sleeboom JJF, van Tienderen GS, Schenke-Layland K, van der Laan LJW, Kruitwagen SA, van Rheenen J, et al. The extracellular matrix as hallmark of cancer and metastasis: from biomechanics to therapeutic targets. Sci Transl Med. 2024;16(728):eadg3840.
19. Nair L, Chung H, Basu U. Regulation of long non-coding RNAs and genome dynamics by the RNA surveillance machinery. Nat Rev Mol Cell Biol. 2020;21(3):123–36.
20. Bhan A, Soleimani M, Mandal SS. Long noncoding RNA and Cancer: a New Paradigm. Cancer Res. 2017;77(15):3965–81.
21. Badowski C, He B, Garmire LX. Blood-derived lncRNAs as biomarkers for cancer diagnosis: the Good, the bad and the Beauty. NPJ Precis Oncol. 2022;6(1):40.
22. Lu J, Xu BB, Zheng HL, Li P, Xie JW, Wang JB, et al. Robotic versus laparoscopic distal gastrectomy for resectable gastric cancer: a randomized phase 2 trial. Nat Commun. 2024;15(1):4668.
23. Lee IS, Lee H, Hur H, Lee SH, Kim SU, Han SU, et al. Transcriptomic profiling identifies a risk stratification signature for Predicting Peritoneal recurrence and Micrometastasis in Gastric Cancer. Clin Cancer Res. 2021;27(8):2292–300.
24. Shimura T, Toden S, Kandimalla R, Toiyama Y, Okugawa Y, Kondo S, et al. Genomewide expression profiling identifies a Novel miRNA-based Signature for the detection of peritoneal metastasis in patients with gastric Cancer. Ann Surg. 2021;274(5):e425–34.
25. Chen D, Liu Z, Liu W, Fu M, Jiang W, Xu S, et al. Predicting postoperative peritoneal metastasis in gastric cancer with serosal invasion using a collagen nomogram. Nat Commun. 2021;12(1):179.
26. Chen Y, Cai G, Jiang J, Zheng J, Xu H, Wang W, et al. Proteomic profiling of gastric cancer with peritoneal metastasis identifies a protein signature associated with immune microenvironment and patient outcome. Gastric Cancer. 2023;26(4):504–16.
27. Sasako M, Sakuramoto S, Katai H, Kinoshita T, Furukawa H, Yamaguchi T, et al. Five-year outcomes of a randomized phase III trial comparing adjuvant chemotherapy with S-1 versus surgery alone in stage II or III gastric cancer. J Clin Oncol. 2011;29(33):4387–93.
28. Strickland MR, Lander EM, Gibson MK, Klempner SJ, Shah MA, Yoon HH. Gastroesophageal adenocarcinomas with defective mismatch repair: current knowledge and clinical management. J Natl Compr Canc Netw. 2024;22(3):e237103.
29. An JY, Kim H, Cheong JH, Hyung WJ, Kim HI, Noh SH. Microsatellite instability in sporadic gastric cancer: its prognostic role and guidance for 5-FU based chemotherapy after R0 resection. Int J Cancer. 2012;131(2):505–11.
30. Lin Z, Song J, Gao Y, Huang S, Dou R, Zhong P, et al. Hypoxia-induced HIF-1α/lncRNA-PMAN inhibits ferroptosis by promoting the cytoplasmic translocation of ELAVL1 in peritoneal dissemination from gastric cancer. Redox Biol. 2022;52:102312.
31. He Q, Yang C, Xiang Z, Xu S, Ding L, Wang Z, et al. LINC00924-induced fatty acid metabolic reprogramming facilitates gastric cancer peritoneal metastasis via hnRNPC-regulated alternative splicing of Mnk2. Cell Death Dis. 2022;13(11):987.